Macromolecules
ARTICLE

Macromolecules **2009**, *42*, 7067–7078 **7067**
DOI: 10.1021/ma9004764

Shear-Enhanced Crystallization in Impact-Resistant Polypropylene Copolymer: Influence of Compositional Heterogeneity and Phase Structure

Shijie Song, Jiachun Feng,* Peiyi Wu, and Yuliang Yang

Key Laboratory of Molecular Engineering of Polymers of Ministry of Education, Department of Macromolecular Science and Laboratory of Advanced Materials, Fudan University, Shanghai 200433, P.R. China

Received March 4, 2009; Revised Manuscript Received August 9, 2009

ABSTRACT: The roles of compositional heterogeneity and phase structure on an unusual shear-enhanced crystallization behavior of impact-resistant polypropylene copolymer (IPC) were systematically investigated by differential scanning calorimetry (DSC), polarized optical microscopy (POM), field emission transmission electron microscopy (FETEM), and scanning electronic microscopy (SEM). Upon an interval of preshearing, we observed an amazing accelerated crystallization in IPC, whereas no such shear-enhanced crystallization was found in isotactic polypropylene (iPP) or iPP/ethylene–propylene random copolymer (EPR) blend after the same shearing. By solvent and thermal fractionation, the effects of components in IPC on shear-enhanced crystallization were clarified. We hypothesize that this phenomenon is a consequence of phase structure changes induced by shearing that releases the partially crystalline block copolymer from amorphous random copolymer which is in favor of a fast crystallization for IPC. We built up a multilayered phase structure of IPC, and by combining the changes in phase structure observed before and after shearing, we present a conceptual model describing the mechanism that account for the significant shear-enhanced crystallization in IPC.

1. Introduction

Polypropylene (PP), owing to its strong mechanical properties, shows a rapid industrial development since its introduction into the market in 1965. A wide range of PP with various molecular characteristics are developed for numerous and versatile applications. PP is widely injected to form parts, especially components such as bumpers and dashboards for the automotive industry. However, because of its poor impact resistance (particularly at low temperatures), PP is unable to optimize the properties of final products which disenable it used as an engineering plastic. Many efforts have been made to improve the toughness of PP,[1−8] among which introducing elastomers by copolymerization is recognized the most effective one. In this field, no great progress has been made until the appearance of porous spherical $TiCl_4$/$MgCl_2$ catalyst and so-called "reactor granule technology" with which made it possible to produce a series of previously unavailable multiphase materials.[9] These materials are named impact-resistant polypropylene copolymer (IPC), high-impact polypropylene (HIPP), or PP in-reactor alloys which exhibit an excellent rigidity–toughness balance. It is believed that the superior properties of IPC originate from its compositional heterogeneity and unique heterophasic morphology as it is produced in-reactor by a multistage polymerization process which involves bulk polymerization of propylene in the first stage and then gas-phased copolymerization of ethylene and propylene in the second stage.[9,10] Extensive investigations have been made to explore the composition, morphology, and phase structure of IPC.[11−17] It has been confirmed that IPC is mainly formed by a matrix of isotactic polypropylene (iPP) in which an ethylene–propylene random copolymer (EPR) is finely dispersed. Besides, some partially crystalline ethylene–propylene copolymers are proved to exist as well.[12] This complex composition suggests the multicomponent and multiphase nature of IPC.

Crystallization is an important physical process in polymer science. Despite decades of research, some fundamental problems in crystallization still remain mysterious for both academe and industry. For semicrystalline polymeric materials such as PP, crystallization proved to be a key factor for final mechanical properties. However, under processing conditions, molten polymer is subjected to an intense shear field and crystallizes during or subsequent to the imposition of shear. Therefore, the crystallization that develops in the product is typically very different from what is observed under quiescent conditions for the same polymer.[18,19] Recently, the influence of shear on the crystallization of PP has drawn much interest[20−30] because it implies the possibility of controlling and predicting the final morphologies and properties in current industrial processes. To understand the effect of shear on crystallization is not an easy task for researchers. Usually, there are two methods to employ shear on molten polymers: (i) By practical processing apparatus such as extruders or laboratory rheometer which provide comparatively higher shear rates.[26,31,32] The influence of shear on crystallization is ex-situ analyzed by differential scanning calorimetry (DSC) or wide-angle X-ray diffraction (WAXD) through which the crystallization kinetics, and possible crystal modification transition can be obtained. (ii) By small handmade shear apparatus combined with in situ analysis techniques such as rheo-optic,[19] rheo-SAXS (small-angle X-ray scattering),[21,33,34] and rheo-WAXD,[22,33,34] a real-time tracking of the crystallization process can be performed. The shear rate of this kind of apparatus is comparatively lower and more controllable, and thus the basic understanding of crystallization under shear is hopeful to be achieved. Concerning

*Corresponding author: Tel 86 21 6564 3735; fax 86 21 6564 0293; e-mail jcfeng@fudan.edu.cn.

Published on Web 08/25/2009

the different responses of various polymers to shear field, both methods own their respective advantages.

Hitherto, a relatively clear overview of crystallization under shear has been given especially for homogeneous polymers such as iPP. The influence of shear condition (e.g., shear temperature, time, and rate) on the subsequent changes in morphology,[20,21] crystal modification,[20] and crystallization kinetics[21,22,34−36] has been well studied. Concerning that the classical problem of shear-induced crystallization is quite extensive; here we focus mainly on the shear-enhanced crystallization in iPP. The shear-enhanced crystallization can be considered as a consequence of shear-induced structure change in polymer melt on the crystallization kinetics and is closely linked to the final property. Thus, an understanding of the nature of shear-enhanced crystallization with respect to the influence of shear conditions and sample characteristics is required to enable rational design of materials and to optimize properties. Using a specific flow apparatus, Kornfield et al.[19,24,25] examined the shear-enhanced crystallization in iPP and found that shearing the polymer for a short duration always led to accelerated crystallization kinetics as compared to quiescent. However, a saturation of shear-enhanced crystallization was also observed, and they suggested that the shear-induced structure formed during shear could explain the phenomenon. They also concluded that the emergence of shear-enhanced crystallization in iPP was related to the shear temperature and polymer characteristic. In brief, shear owns the ability to induce more active nuclei in iPP melt and shorten the induction time. However, from a macro-perspective, the shear-enhanced crystallization in iPP cannot always be observed due to some uncertain reasons. All the related factors such as shear condition and molecular characteristic should be taken into consideration if a shear-enhanced crystallization is expected. Therefore, the origin of shear-enhanced crystallization is still ambiguous, and relevant studies are in progress.[37−39]

As a typical multicomponent and multiphase polymer, the understanding of shear-enhanced crystallization in IPC is more complicated than iPP because it may be related to not only shear but also the phase sturcture.[15,40−43] In our pervious study,[44] we reported an experimental study about the influence of preshearing on the crystallization of IPC and first showed that the preshearing greatly accelerated the crystallization rate of IPC. However, to the best of our knowledge, no similar shear-enhanced crystallization of iPP has been reported under the same shear condition. Upon shearing, the possibility of forming shear-induced structure ought to exist in both IPC and iPP. However, because of some other unknown reasons, the resultant enhancing effects appear to be very different. Therefore, a simple but "big" question naturally arises as to why the crystallization of iPP and IPC, both of which have propylene homopolymers as the main constitute, behave so differently after shear. The possible mechanism of shear-enhanced crystallization in IPC is expected to be revealed.

Using the shear-enhanced crystallization in IPC as a start point, the aim of this study is to give out a reasonable mechanism to explain the interesting phenomenon, which might be helpful for the better understanding of the shear-enhanced crystallization in complex systems. First, we applied a preshearing process on iPP, iPP/EPR, and IPC by a torque rheometer to study the shear-enhanced crystallization. Then, for a more detailed analysis, IPC samples were separated by solvent and thermal fractionation. The functions of different components in shear-enhanced crystallization were well investigated. We also built up a complete multilayered phase structure of IPC based on the observation using scanning electron microscopy (SEM), field emission transmission electron microscopy (FETEM), and selective area electron diffraction (SAED). The thermal properties and crystalline morphologies were analyzed by DSC and polarized optical microscopy (POM), respectively. On the basis of the results obtained and through substantial analysis, we proposed a model to explain the possible mechanism of shear-enhanced crystallization in IPC. Some experiments were also conducted to testify our model.

Table 1. Properties of IPC, iPP, and EPR

sample	comonomer type	MFI[a] (g/10 min)	ethylene content[b] (%)	M_w[c] ($\times 10^4$)	M_w/M_n[c]
IPC	ethylene	9.7	10.6	15.3	5.02
iPP		2.5		22.0	4.85
EPR	ethylene		50.6	8.6	< 2.30

[a] Under the condition of 230 °C/2.16 kg. [b] Determined by ^{13}C NMR. [c] Determined by gel permeation chromatography (GPC).

2. Experimental Section

2.1. Experimental Materials. The IPC and iPP used in the present study are commercial products with granule forms produced by Qilu Petrochemical Co., SINOPEC (Shandong, China), and Yangzi Petrochemical Co., SINOPEC (Nanjing, China), respectively. The EPR is provided by Jilin Petrochemical Co., CNPC (Jilin, China). The basic parameters of the materials are summarized in Table 1. iPP/EPR is produced by melt-blending with an EPR content of 20 wt %.

2.2. Sample Preparation. Preshearing was carried out by a PLE 651 torque rheometer (Brabender, Germany) to simulate the practical industrial processing. The parameters of the rheometer and corresponding experimental procedures were described in our previous study.[44] In the present study, a rotor speed of 40 rpm (γ = 44.0 s^{-1}) and a duration time of 10 min were applied at a temperature of 175 °C. We have carefully studied the possible degradation and cross-linking of the samples after preshearing, and the results showed that under the shearing conditions used in the present study no obvious degradation or cross-linking will happen in IPC samples, and therefore, it can be confirmed that these factors will not influence our study of shear-enhanced crystallization. The detailed studies and discussions are available in the Supporting Information.

Solvent fractionation was performed according to the following procedures; First, IPC pellets were totally dissolved in boiling xylene containing 0.1 wt % antioxidant. The homogeneous solution was then cooled to room temperature and washed by large amounts of cold methanol. After filtration, the obtained IPC in the form of powders were subsequently fractionationed by *n*-hexane. The fraction dissolved in *n*-hexane was washed out by methanol. Schematic illustration of solvent fractionation is shown in Figure 4. All the fractions were dried in vacuum for 24 h before testing.

2.3. Thermal Analysis and Thermal Fractionation. A Mettler DSC-1 apparatus was used to determine the thermal properties. Calibration for the temperature scale was performed using indium (T_m = 156.60 °C and ΔH_f^0 = 28.45 J/g) as standard to ensure reliability of the data obtained. The accuracy of temperature measured here is ±0.05 °C. All the experiments were carried out in a nitrogen atmosphere. Each sample weighted about 2−5 mg and was sealed in aluminum pan. For regular melting and crystallization analysis, the measurements were performed as following procedures: samples were heated to 200 °C and kept for 5 min to erase previous thermal history. Subsequently, the samples were cooled to 25 °C at a rate of 10 °C/min and again heated to 200 °C at a rate of 10 °C/min. The crystallization thermograms were recorded during the first cooling scan, while the melting temperature and fusion enthalpy of the samples were determined during the second heating scan.

Successive self-nucleation and annealing (SSA) was performed according to the following procedures; samples were first held at 200 °C for 5 min and then cooled to 25 °C at a rate of 10 °C/min to create an initial "standard" thermal history.

Second, samples were heated to a selected first self-seeding temperature (T_s) at a rate of 10 °C/min and held for 5 min. This step results in partial melting and annealing of unmelted crystals, while some of the melted species may isothermally crystallize. Crystallization after self-nucleation was achieved by subsequently cooling samples to 25 °C at a rate of 10 °C/min. Following the suggestion of Muller,[45] single-step self-nucleation experiments have been done to determine the melting domains of samples. In the present study, the first T_s was determined to be 180 °C, the fraction window adopted here was 5 °C, and the annealing time was 5 min. The scanning rate used during the thermal conditioning steps was 10 °C/min. The temperature range for thermal fractionation was from 180 to 50 °C for all samples. After the completion of thermal fractionation process, samples were heated from 25 to 200 °C at a rate of 10 °C/min, and the corresponding endothermic curves were recorded.

2.4. Scanning Electron Microscopy (SEM). The samples were hot-pressed into films and then carefully etched in a mixed solution of $KMnO_4$, hydrochloric acid, and concentrated sulfuric acid. A scanning electron microscopy (TESCAN 5136MM) was used to observe the surface of samples after coated with gold. An operating voltage of 20 kV and magnification of 800, 2000, and 5000 were adopted for observation.

2.5. Field Emission Transmission Electron Microscopy (FETEM). The as-received IPC sample was dissolved in boiling xylene (138 °C) with a concentration of 0.05 wt %. Thin films (thickness < 200 nm) for observation were prepared by solution-casting to a preheated copper grids. After solvent evaporation, the specimens were then dried in vacuum at 50 °C for 24 h. A JEM-2100F (JEOL, Tokyo, Japan) field emission transmission electron microscopy operated at 200 kV was used for observation.

2.6. Polarized Optical Microscopy (POM). Morphological evolution during isothermal crystallization was observed using an Olympus BX-51 polarized optical microscope with a Linkam-THMS600 hot stage. The sensor accuracy of the hot stage is ±0.1 °C. Samples were melted at 200 °C and squeezed to films tenderly. These film specimens were kept in hot stage between two microscope slides. Each specimen was heated to 200 °C and kept for 5 min to allow complete melting and subsequently cooled to a predetermined isothermal crystallization temperature at a rate of 40 °C/min. Nitrogen gas was purged through the hot stage during measurements.

2.7. Dynamic Mechanical Analysis (DMA). DMA was conducted using a NETZSCH 242C dynamic mechanical analyzer. Specimens with approximate dimensions of 10.0 × 5.0 × 2.0 mm^3 were carefully cut from the bone-shaped bars prepared by a laboratory mixing molder (LMM). Dynamic temperature sweep were performed using single-cantilever mode at a vibration frequency of 10 Hz under a nitrogen atmosphere. The testing temperature was selected from −60 °C to +80 °C at a heating rate of 5 °C/min.

3. Results and Discussion

3.1. Thermal Properties. In our previous study,[44] we found the crystallization behavior of IPC is sensitive to strong shear employed by a torque rheometer. With various shear rates, the overall crystallization kinetic of presheared IPC can be improved to different extents. In the present study, we further studied the same material to look insight into the possible mechanism of shear-enhanced crystallization in IPC. For comparison, we selected three polypropylene samples including iPP, iPP/EPR blend, and IPC. The samples were undergone an identical melt shearing at a rate of 44.0 s^{-1} for 10 min at 175 °C by a Brabender rheometer. It should be noted that the choice of shear rate, duration time, and temperature of shearing has an influence on the shear-enhanced crystallization. Under critical conditions, the shear-enhanced crystallization reaches saturation in IPC.

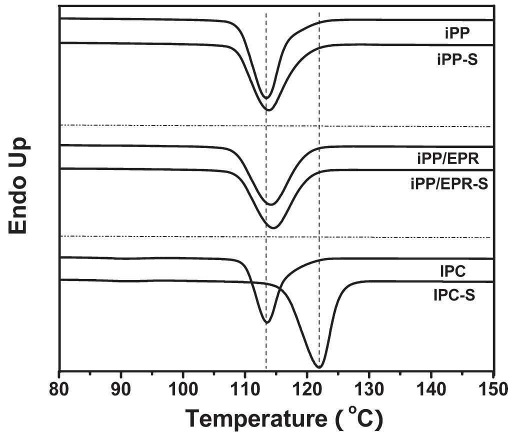

Figure 1. DSC crystallization curves of iPP, iPP/EPR, and IPC samples.

The shear condition employed here has been proved to be a critical one leading a maximum enhanced crystallization in IPC. The presheared samples were denoted as iPP-S, iPP/EPR-S, and IPC-S. Figure 1 shows the crystallization curves of three samples before and after preshearing. The peak value of crystallization curve, T_p, can be used as a parameter which links to the crystallization rate of semicrystalline polymer. From Figure 1, it can be seen that the T_p of iPP-S was 113.8 °C, only 0.3 °C higher than that of iPP, indicating that the preshearing we applied here did not cause obvious shear-enhanced crystallization in iPP samples. In the case of iPP/EPR, still no obvious elevation of T_p was found in the crystallization curve. Nevertheless, given the results of IPC and IPC-S, it is interesting to find that the T_p of IPC-S was elevated from 113.5 to 122.1 °C, almost 9.0 °C higher than that of IPC. Our previous crystallization kinetic analysis[44] has shown that the half-time of crystallization ($t_{1/2}$) of IPC sample with a similar elevated T_p could be shortened by about 1 magnitude during isothermal crystallization under 129.0 to 135.0 °C. Thus, the great elevation of T_p in IPC should be associated with an unusual faster crystallization rate.

It should also be noted here that we found the shear-enhanced crystallization in IPC can be eliminated by a series of annealing procedures. Many researchers believed that the shear-enhanced crystallization is related to the orientation of some polymer chains (especially high molecular weight polymer) and will undergo a recovery process to its original.[18,19,21,22,24,25,33,46−51] Given different polymer samples, the relaxation process may last for different times. According to the time−temperature correspondence, if the polymer is kept in a high temperature atmosphere, the relaxation process may be easier to observe and record. Figure 2 presents the crystallization curves of IPC-S samples after annealing at various temperatures for 30 min. It is interesting that the relaxation process was noticeable and showed a dependence of annealing temperatures. The higher the annealing temperature we adopted, the faster the relaxation we observed. When the annealing temperature set to 230.0 °C, the T_p of the IPC-S sample after annealing was nearly identical to that of IPC, indicating that a sufficient relaxation was achieved and the preshearing memory was totally erased.

The results above led us to the conclusion that in spite of the same main constituent, polypropylene, the crystallization behaviors of iPP, iPP/EPR, and IPC gave different responses to external shear. Relatively speaking, the crystallization of IPC exhibited a much stronger response to shear

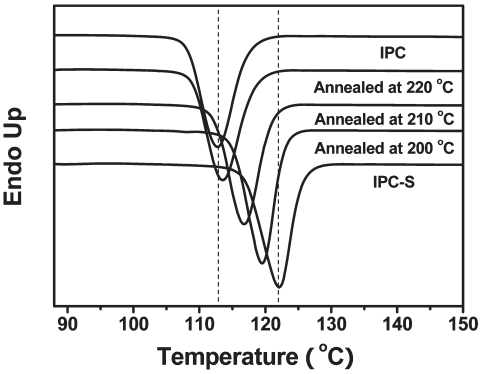

Figure 2. Crystallization curves of IPC-S samples after annealing at various temperatures for 30 min.

than iPP and iPP/EPR. Moreover, the resultant shear-enhanced crystallization appeared to be reversible by annealing procedures. If taking iPP and IPC for comparison, one may suspect that the reason for their different responses to shear lies in the presence of EPR. However, this simple explanation cannot tell us why iPP/EPR blend with same ethylene content to IPC did not show a shear-enhanced crystallization. As the addition of EPR was not the key fact, it is natural for us to consider other differences between iPP/EPR and IPC. As far as we know, the unique polymerization process determines the particularity of IPC in its composition and phase structure. On the one hand, the partially crystalline block copolymers, which are absent in iPP/EPR blend, do exist in the IPC system.[12,40] On the other hand, the extraordinary property of IPC indicates its special phase structure compared with iPP/EPR blend. Therefore, we may expect that the reason for this uncommon shear-enhanced crystallization lies in the two aspects. Apparently, in order to reveal the mechanism behind, the effects of different components in IPC on crystallization should first be well investigated.

3.2. Solvent and Thermal Fractionation. It is well-known that, for multicomponent polymer systems, solvent fractionation is an effective way to separate the different components. In the case of IPC system, if a carefully solvent fractionation is carried out, the dispersed amorphous phase and the crystalline phase can be totally separated. A pretreatment procedure was used here before solvent fractionation. We first dissolved the IPC granules by xylene at a temperature of 130 °C for a sufficient time. The homogeneous solution containing IPC was cooled down to room temperature and washed by large amounts of methanol. After filtration, the IPC were collected in the form of powders. The purpose of this treatment will be stated as below. In the present study, we aimed to totally remove the amorphous components (e.g., ethylene−propylene random copolymers) in IPC. However, the as-received IPC samples are in the form of pellets with diameters of several millimeters. According to a previous study,[14] most amorphous components in IPC particles are finely dispersed in PP subglobes with diameters of several microns, which means it is difficult to totally remove the amorphous components directly from IPC pellets during fractionation. Therefore, we designed this pretreatment by dissolving the sample into xylene and then precipitated by cold methanol. As a result, the obtained samples were in the form of fine powders, and using these powders for further solvent fractionation will certainly help to totally remove the amorphous component. We have compared solvent fractionations by using IPC pellets and pretreated IPC powders, and the result has been showed in the Supporting Information.

Table 2. Quantities of the Soluble and Insoluble Component in IPC after Solvent Fractionation

number	feeding (g)	insoluble (%)	soluble (%)	recovery rate (%)
I	2	76.94	19.28	96.22
II	2	77.80	18.26	96.06
III	2	77.33	18.99	96.32
average	2	77.36	18.84	96.20

The obtained powders were further fractionationed by *n*-hexane to a thorough separation between the amorphous and crystalline component. The insoluble and soluble fraction, corresponding to amorphous component and crystalline component, were both dried in vacuum before other measurements. We repeated the solvent fractionation three times, and the quantities of the insoluble and soluble fractions are provided in Table 2.

Figure 3 shows the thermal properties of as-received IPC and solvent fractionated IPC samples as well as the schematic illustration of solvent fractionation. As expected, the DSC curve of the soluble fraction showed no obvious peaks in either endothermic curve or exothermic curve, indicating that the soluble fraction was consisted of amorphous components. To confirm whether the amorphous component was totally removed from IPC sample, we performed a DMA measurement for both IPC and insoluble fraction of IPC as shown in Figure 4. A distinct difference can be found between the two samples. In the case of IPC, it is clear that two obvious peaks appeared with the increasing testing temperature. Concerning the composition and chain structure of IPC, the peak at lower temperature and the peak at higher temperature can be recognized as the glass transition of amorphous random copolymer and polypropylene homopolymer, respectively. However, for the insoluble fraction of IPC, it can be seen that the peak at lower temperature totally disappeared whereas the peak at higher temperature was elevated several degrees higher compared with IPC. Two conclusions could be judged from the results of DMA. One is, by solvent fractionation, the amorphous component has been completely removed from IPC system. The other is, in the IPC sample, a strong combination existed between the dispersed phase and the matrix which could be inferred from phenomenon that the glass transition temperature of polypropylene component in IPC moved to a lower value closer to that of amorphous random copolymer. Usually, this phenomenon can be considered as a sign of improved compatibility between the two components.

Looking back to the results of Figure 3, the melting curve of the insoluble fraction of IPC was similar to that of IPC. Only one obvious endothermic peak at about 170.0 °C corresponding to the melting of polypropylene can be found. However, with regard to the crystallization curve, it is surprising for us to find that the T_p of insoluble fraction was greatly elevated from 113.5 to 122.2 °C. In other words, after removing the amorphous component, the IPC sample exhibited a very similar crystallization behavior to IPC-S; that is to say, the crystallization kinetics of insoluble fraction was also greatly accelerated. An even more surprising result was obtained when we applied an annealing procedure to the insoluble fraction of IPC. Figure 5 shows the crystallization curves of both the insoluble fraction of IPC and IPC-S samples before and after annealing at 220 °C for 60 min. It can be seen that the T_p of IPC-S sample totally recovered to its original value which is the same as IPC sample. However, for insoluble fraction of IPC sample, though treated by the same annealing procedure, the crystallization curve did not exhibit any changes. Therefore, it can be said that the accelerated crystallization behavior of insoluble fraction of IPC is irreversible or perpetual.

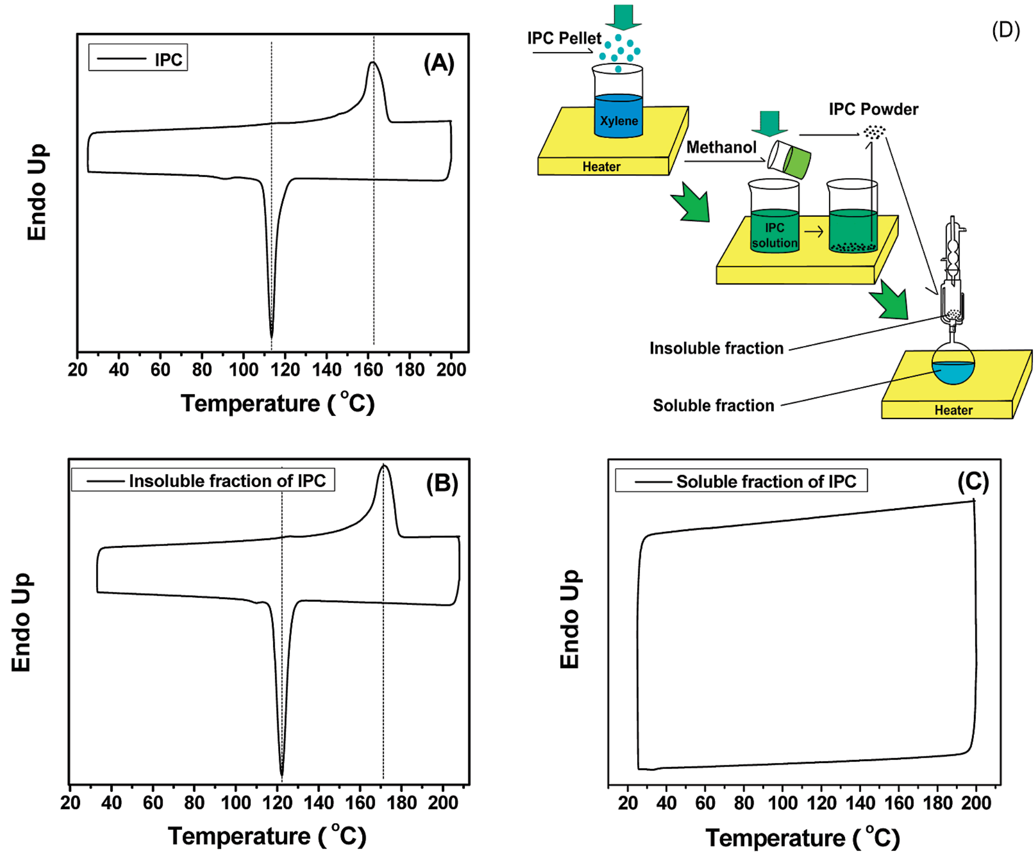

Figure 3. DSC thermograms of IPC (A), insoluble fraction of IPC (B), and soluble fraction of IPC (C) and schematic illustration of solvent fractionation (D).

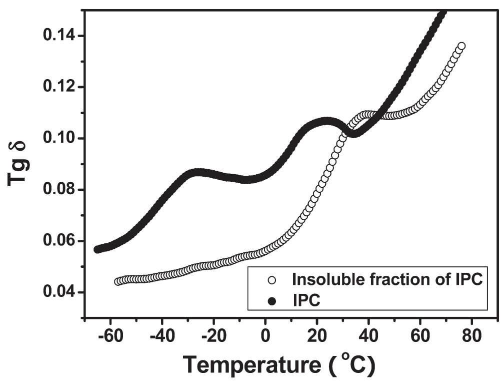

Figure 4. DMA curves of IPC and insoluble fraction of IPC.

Because of the above unexpected crystallization behavior of IPC after removing the amorphous component, we tried to further explore the composition of the insoluble fraction of IPC by SSA thermal fractionation. SSA thermal fractionation enhances the potential molecular fractionation which can occur during crystallization, while encouraging annealing of the unmelted crystals at each stage of the process, so that small effects can be magnified. This technique is based on the sequential application of self-nucleation and annealing steps to a polymer sample originally designed and first reported by Muller et al.[45,52,53] and has been widely used to analyze the chain structures of semicrystallized polymers such as PE and PP.[54−58] For a SSA fractionated polymer sample, the final DSC heating run will reveal a distribution of melting points induced by thermal treatment, indicating the heterogeneous nature of the structures of polymers, which is hard achieve by solvent fractionation. Figure 6 shows the DSC endotherms of IPC and insoluble fraction of IPC after SSA treatment. The series of melting peaks observed in the DSC heating scans indicate that thermal fractionation has occurred during the SSA treatment. The fractions that exhibit higher melting points in Figure 6B are crystalline polypropylene segments. Both samples exhibited two separated melting peaks, one strong peak at about 171 °C and one shoulder peak at about 177 °C, indicating the existence of two crystal lamellas with different thickness. Comparatively, the proportion of thinner crystal lamellas in insoluble fraction is a little larger than that in IPC. In other words, the insoluble fraction of IPC is more inclined to form thinner lamellas. It is interesting to see that at lower temperature both IPC and insoluble fraction of IPC exhibited a series of melting peaks. According to the principle of the SSA method, only those components with structural heterogeneity will show a serial of melting peaks after thermal fractionation. Thus, these melting peaks can be attributed to be the melting of crystalline segments with different length in ethylene−propylene block copolymer. One may notice that in Figure 6A the peaks after solvent fractionation became a little smaller; by analyzing the possible reasons, we give our interpretation below. Solvent fractionation we employed here involves two steps: (1) dissolving IPC in boiling xylene and precipitation with cold methanol; (2) fractionation by hot *n*-hexane. We aimed to totally remove amorphous component in IPC; however, it cannot be denied that there lies the possibility of the loss of a few crystalline components during the fractionation. In IPC, there exists crystalline PP, partially crystalline ethylene−propylene block copolymer, and crystalline PE. Compared with crystalline PP segments, crystalline PE segments are more inclined to dissolve in the solvent during fractionation. Therefore, the peaks after

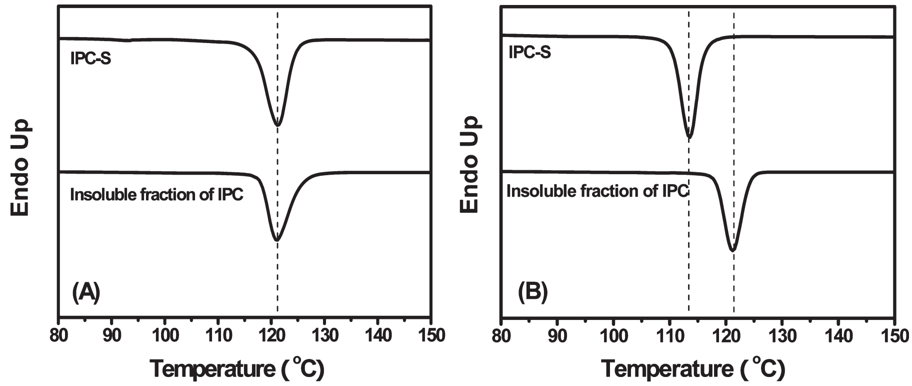

Figure 5. Crystallization curves of IPC-S and insoluble fraction of IPC before (A) and after annealing (B).

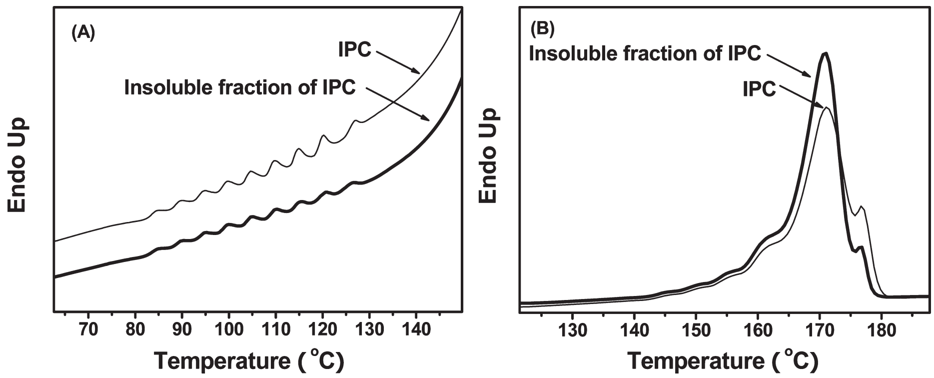

Figure 6. DSC endotherms of IPC and insoluble fraction of IPC after SSA treatment: (A) low-temperature fraction and (B) high-temperature fraction.

fractionation corresponding to the crystalline PE segments will become smaller. However, the phenomenon will not alter our conclusion that after fractionation the ethylene–propylene block copolymer still existed in IPC because only those components with structural heterogeneity, for example, ethylene–propylene block copolymer with different crystalline segments length in the present study, will show a serial of melting peaks after thermal fractionation. In other words, completely linear polyethylene or high isotactic polypropylene cannot be thermal fractionationed by the SSA method. Therefore, the results of thermal fractionation in our study still proved the existence of ethylene–propylene block copolymer from another aspect.

A real time observation of the crystalline morphological evolution of IPC, IPC-S, and insoluble fraction of IPC during isothermal crystallization was also performed by POM equipped with a hot stage (Figure 7). The isothermal crystallization was conducted at 135 °C. At the beginning of isothermal crystallization (1 min), the IPC sample, as shown in Figure 7A, remained a homogeneous phase in which almost no nuclei could be observed. However, with regard to the IPC-S and insoluble fraction of IPC, as shown in Figure 7B,C, some sporadic nuclei were already visible, indicating a much earlier germination. At 5 min, it was clear that some nuclei emerged and began to grow in the IPC sample while in the other two samples the germination of nuclei and the growth of crystals were so rapid that the screen had already been full of spherulites which began to impinge on each other. After 10 min of isothermal crystallization, it can be seen that no more nuclei appeared in IPC sample and the formed spherulites began to grow radially. For IPC-S and insoluble fraction of IPC, the crystallization had already gone to saturation at 10 min. Under the same crystallization temperature, the number of nuclei formed during a limited crystallization time may represent the nucleation rate of the sample. Therefore, it is clear that the nucleation rate of both IPC-S and insoluble fraction of IPC showed a similarly significant promotion compared with IPC.

The crystallization morphologies of IPC and insoluble fraction are spherulitic while it is quite difficult to distinguish whether the IPC-S is the same case due to its small entity size. Therefore, we conducted an isothermal crystallization at 150 °C for IPC-S because at higher temperature, the crystals tend to grow bigger. The result showed that both perfect spherulites and less perfect spherulites can be observed. Concerning that in IPC-S sample, the amorphous component still existed, and the preshearing may result in a certain degree of heterogeneity in phase distribution; therefore, some crystals cannot grow to perfect spherulites. However, to a large extent, the nuclei are randomly distributed in the sample and induce a spherulitic growth which is consistent with previous study.[59] Moreover, some PP crystals of beta-modification were also found in IPC-S using wide-angle X-ray diffraction (WAXD) corresponding to the brighter entities in Figure 7B. The POM micrograph taken at 150 °C and the results of WAXD measurement are available in the Supporting Information.

In brief, with all the results above, we could reach the following conclusions. First, the insoluble fraction of IPC showed a similar enhanced crystallization behavior to IPC-S. The POM observation confirmed the existence of a fast nucleation and crystal growth rate of the insoluble fraction. Second, the partially crystalline ethylene–propylene block copolymers have been proved to exist in insoluble fraction of IPC and own the possible ability in improving the nucleation of polypropylene. Third, unlike IPC-S, the accelerated crystallization in the insoluble fraction turned out to be irreversible. Combining these conclusions, we may get

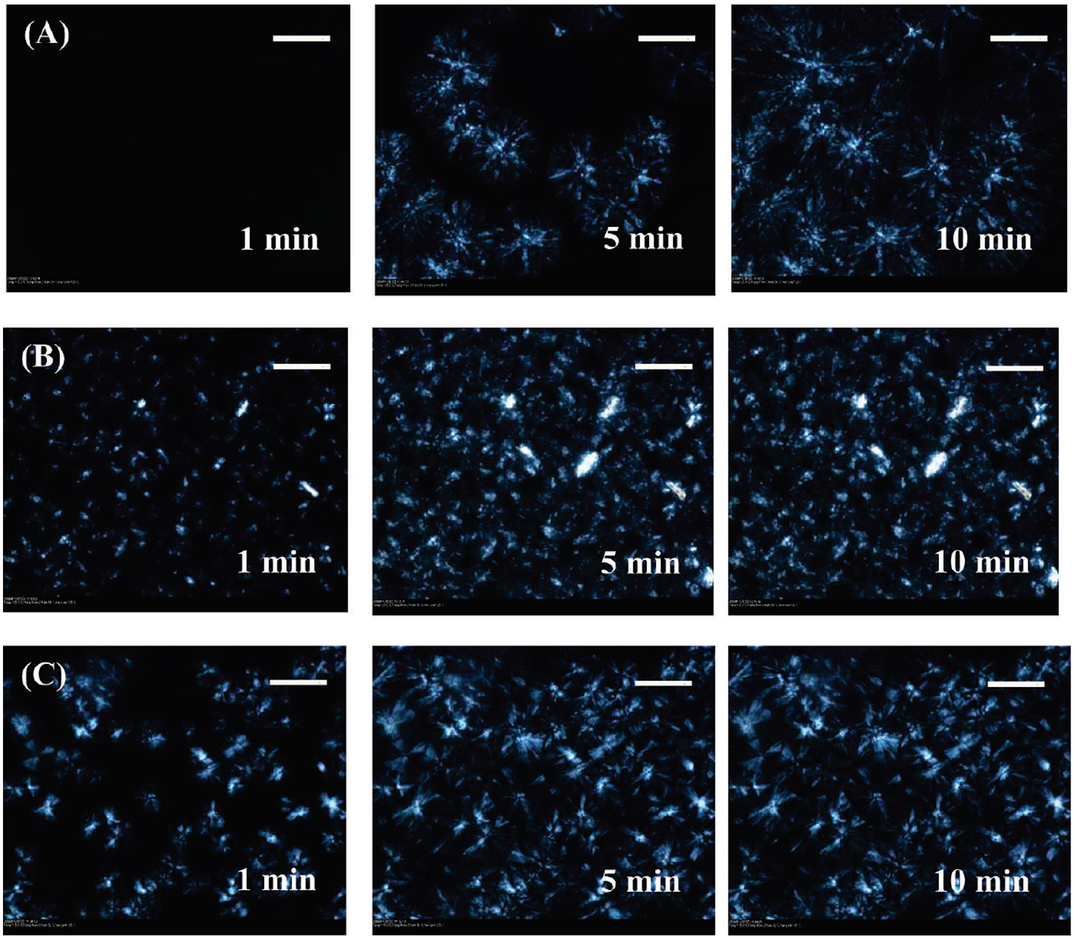

Figure 7. Crystalline morphological evolution of IPC (A), IPC-S (B), and insoluble fraction of IPC (C) during isothermal crystallization. The white bar represents 10 μm.

a better understanding about the shear-enhanced crystallization in IPC; that is, the partially crystalline block copolymers tend to be able to improve the crystallization, and however, because of the existence of the amorphous random copolymers, this ability is suppressed. In other words, a mutual interaction between the two components is thought to be exist. With the appearance of shear, the interaction is affected to some extents, which can be reflected on the crystallization behaviors.

3.3. Phase Structure. In order to further illustrate mentioned interaction between partially crystalline copolymer and the amorphous random copolymer, we observed the phase morphologies of both IPC and IPC-S using SEM. The two samples in the form of films were carefully etched at room temperature. With an appropriate etching time, the amorphous components can be removed while the crystalline components can be preserved. Figure 8 contains the SEM micrographs of the surface of both samples at different magnifications. It can be seen that both samples exhibited obvious microscopic phase separation, and the dimensions of the dispersed globular phase, which can be recognized as random copolymers, are all about 1−2 μm. However, a distinct difference between the two groups of photographs can also be observed. For IPC sample (Figure 8A), except for the dispersed phase, many stripe-shaped phases were also etched. Given higher magnifications, clearer phase morphology showed that the stripe-shaped phases in IPC were distributed around the etched amorphous phase and connected by the amorphous phase and the matrix. Whereas in the case of IPC-S sample, there existed only amorphous phase and the matrix; no stripe-shaped phases could be observed. Obviously, it is necessary to interpreter the origin of the stripe-shaped phase observed. Therefore, referred to a recent work by Yang et al.,[16] we conducted some experiments using field-emission transmission electron microscopy (FETEM) to build up a clearer concept of the multiphase structure and corresponding constituents in IPC. Figure 9A shows the micrograph of IPC sample without any thermal treatment. From Figure 9A, it can be seen that some gray stripes which can be attributed to the crystalline PP segments are growing out from a dark spherulitic region. The selective area electron diffraction (SAED) presented in Figure 9A show that in the core of the dark region the pattern can be recognized as the characteristic orthorhombic crystal of PE. However, when we selected the fringe area of the dark region for electron diffraction measurement, six symmetrical diffraction points corresponding to the hexagonal crystal structure of PE can be observed. Usually, the hexagonal structure forms only under high-pressure crystallization condition. Concerning the IPC sample here was crystallized from dilute solution, we attributed the hexagonal crystal to the crystallization of PE segments of crystalline ethylene−propylene block copolymer in IPC. Recently, some studies[16,60−62] have shown that some crystalline short PE segments of ethylene−propylene block copolymer can form hexagonal crystal under normal conditions. Therefore, it is confirmed from Figure 9A that in IPC there exists the crystalline ethylene−propylene block copolymer whose PP segments can crystallized into the matrix and PE segments can also form a crystalline-rich phase. However, when we applied a thermal

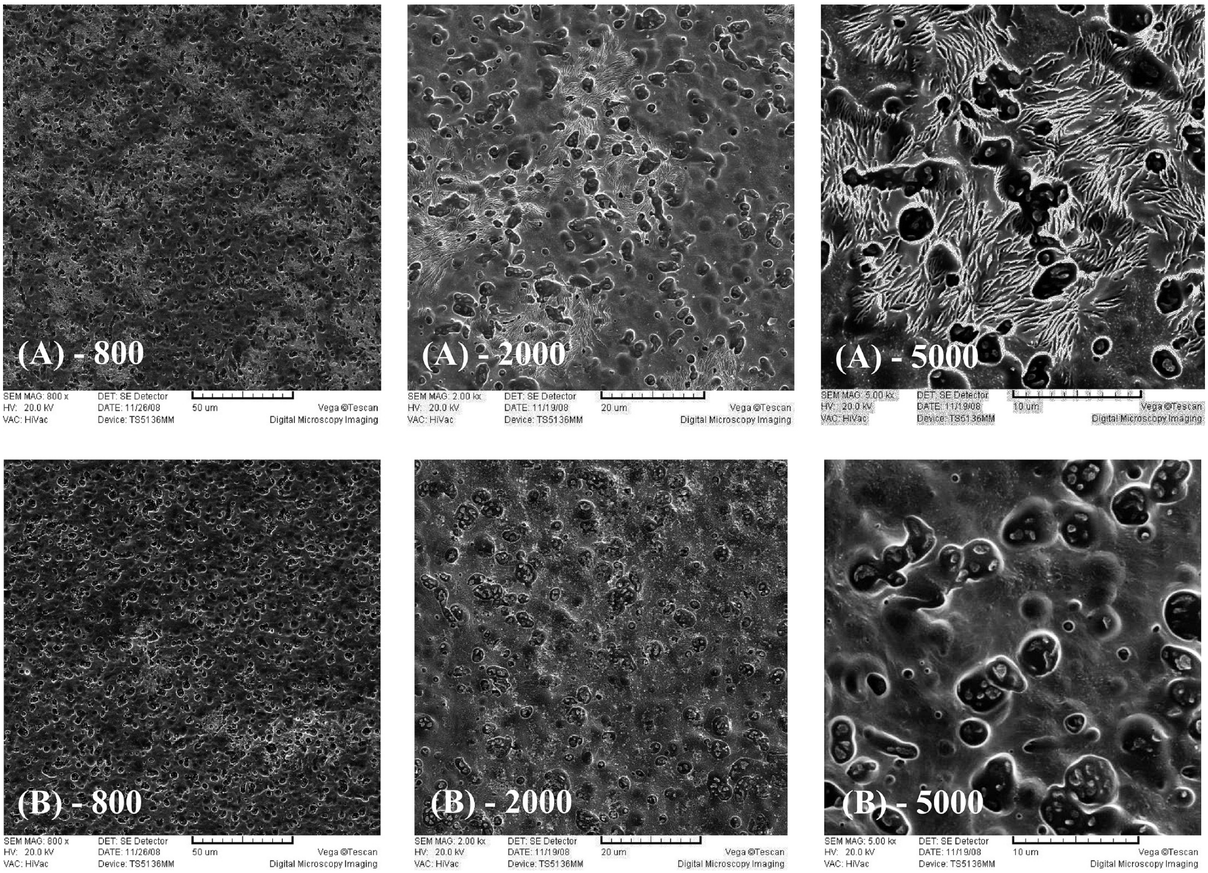

Figure 8. SEM micrographs of IPC (A) and IPC-S (B) at different magnifications.

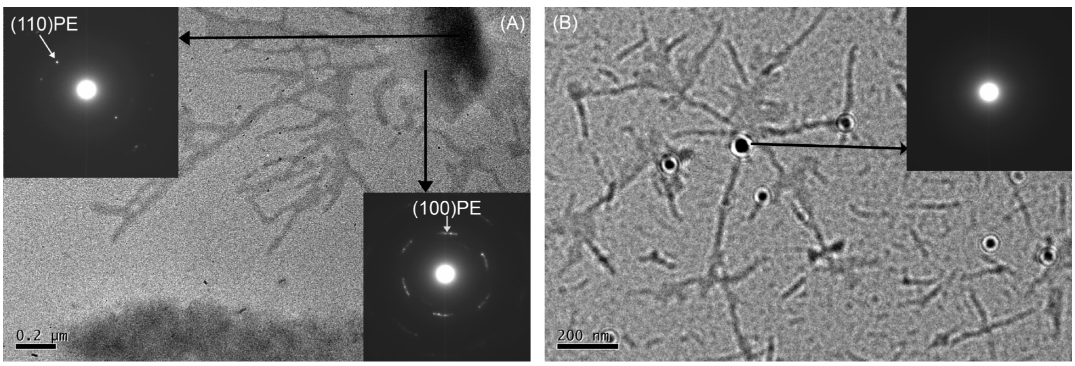

Figure 9. FETEM and selective area electron diffraction (SAED) of as-received sample before (A) and after thermal treatment (B).

treatment (heated to 200 °C and then isothermally kept at 140 °C for 2 h) to the same sample before observation, we found a spontaneous self-assembly of IPC melt happened. The dispersed spherulitic phases with clear multilayered core–shell structure appeared as shown in Figure 9B. It can be seen that the multilayered core–shell structure is composed of the black core area, the white middle layer, and the black thin outside layer with relative low contrast. The core was attributed to the crystalline PE with characteristic orthogonal crystal as we have shown in Figure 9A. The white middle layer, as the SAED showed only diffused circles, can be recognized as the amorphous ethylene–propylene random copolymer. The thin outside layer was composed of crystalline ethylene–propylene block copolymer from which some PP crystals were grown out.

A more clear and integrated phase morphology of as-received IPC has been presented in Figure 10, and a magnified particle showing the location of each composition has also been given. In the magnified particle, the dark area marked by arrow 1 exhibiting the strongest contrast is mainly composed of PE homopolymers because the SAED result of this area as we have provided showed that the core was attributed to the crystalline PE with characteristic orthogonal crystal. The white area marked by arrow 2 exhibiting the weakest contrast is composed of ethylene–propylene random copolymers because the SAED result showed only diffused circles indicating that the area is amorphous. The fringe area with weaker contrast compared to the core area marked by arrow 3 can be regarded as ethylene–propylene block polymer. The SAED result of this area showed a characteristic hexagonal crystal structure of PE which can be formed by some crystalline short PE segments of ethylene–propylene block copolymer. Moreover, the area marked by arrow 4 seems to link with fringe area which confirms that in IPC there exists the

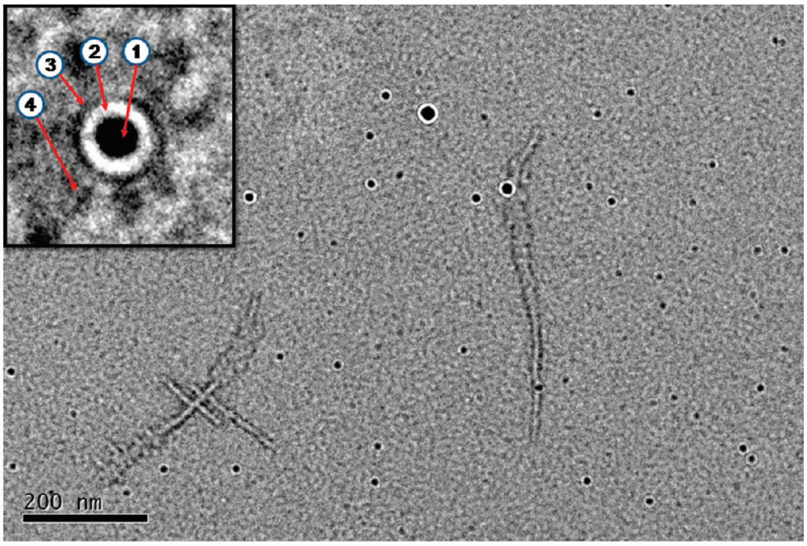

Figure 10. Multilayered phase morphology of IPC and the location of each component.

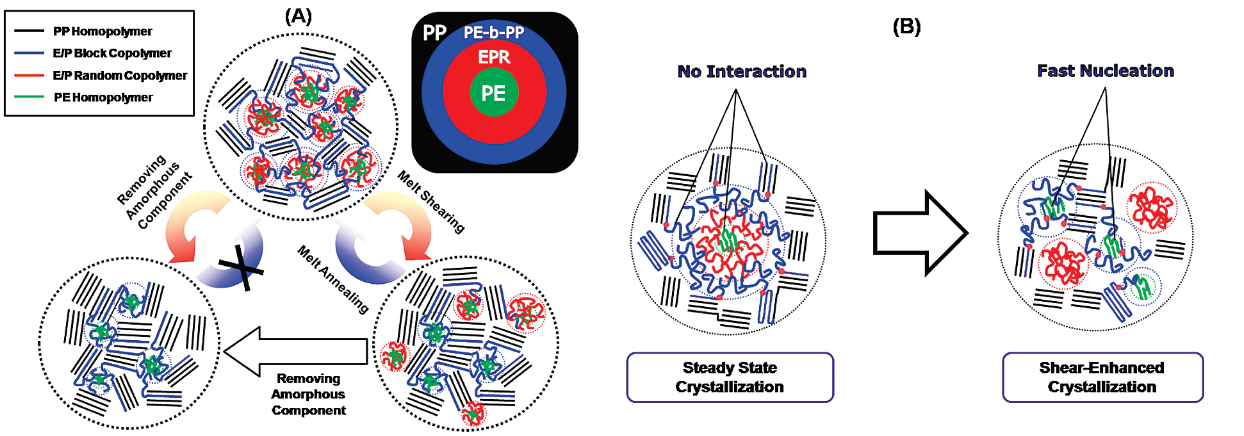

Figure 11. Schematic model depicting phase transition after preshearing and solvent fractionation (A) and shear-enhanced crystallization (B) in IPC.

crystalline ethylene–propylene block copolymer whose PP segments can crystallized into the matrix and PE segments can also form a crystalline-rich phase. The unique multilayered phase structure can largely account for the superb mechanical property of IPC.

From the above results of FETEM, we have gained a clear concept about the hierarchical phase structure in IPC. Therefore, we can turn back to the stripe-shaped phases observed in SEM and give a reasonable explanation. The IPC samples used in FETEM observation were crystallized from dilute solution with very low concentration while the samples used in SEM observation were crystallized from melt which means from a very high concentration environment. Therefore, it can be understood that the scale of the phase structure observed in SEM is much larger than that in FETEM because when the concentration increases, the different constituents in IPC will aggregate, redistribute, and assemble to a similar phase structure but with larger scale. That means despite the different scales in FETEM and SEM, the phase structure observed owns a similarity to a large extent. For the as-received IPC sample, the partially crystalline ethylene–propylene block copolymers are enriched around the outside layer of the dispersed phase; some parts of them can grow into a crystalline PP matrix while some parts of them are trapped by the chains of amorphous component. Therefore, the flexibility of the crystallizable segments is decreased, and as a result, the formed crystals are imperfect and can be etched, leading to the appearance of stripe-shaped phases in the SEM micrograph. On the other hand, when the preshearing applied in IPC, as we can see from the SEM micrographs, the stripe-shaped phases disappeared, indicating a possible damage of original phase structure due to the stress field. The interaction between ethylene–propylene block copolymer and amorphous component was destroyed, and the crystallizable segments of block copolymer therefore formed more perfect crystals which cannot be etched under the same conditions. Concerning that the shear-induced changes in phase structure were accompanied by a shear-enhanced crystallization, we may expect that a possible correlation should exist between the two phenomena.

3.4. Model Assumptions. On the basis of the observed experimental phenomena, we proposed a conceptual model to explain the mechanism of shear-enhanced crystallization in IPC as shown in Figure 11. For a better understanding, a schematic description of the multilayered phase structure of IPC is also provided in the figure. In Figure 11A the upper-middle globe describes the quiescent phase structure of as-received IPC sample. The structure appears to be macroscopically homogeneous but microscopically phase-separated. The dispersed phase owns a typically multilayered structure. The core area of the dispersed phase is composed of PE homopolymers, the middle area is composed of ethylene–propylene random copolymers, and the outside fringe area is composed of ethylene–propylene block copolymers. The dispersed phases scatter like islands with different dimensions in the ocean consisted of a crystalline PP matrix. The excellent balance between the toughness and rigidity of IPC is attributed to the effect of the partially crystalline ethylene–propylene block copolymers which work as a bridge connecting the amorphous enriched phase and crystalline enriched matrix as shown in Figure 11A. Because of the chemical similarity, the crystallizable PP segments of the block copolymer could take part in the crystallization of polypropylene while the some crystallizable PE segments were twisted together with the chains of amorphous phase. Thus, the compatibility between the two phases is greatly improved by the presence of the block copolymer.

The globe located lower-right in Figure 11A illustrates the phase structure of IPC-S sample. In the model, it can be seen that if the shear applied to the molten IPC is sufficiently large, the crystallizable PE segments which twisted with the amorphous phase can be pulled out and gather together to form tiny dispersed particles. Figure 11B exhibits a more detailed process of the steady-state crystallization and shear-enhanced crystallization in IPC. As shown in Figure 11B, under the condition of steady state, the crystallization of PE homopolymers has no interaction with the crystallization of ethylene–propylene block copolymers as well as the PP homopolymers due to the existence of ethylene–propylene random copolymers located between them. This specific multilayered phase structure has been well presented by FETEM as we have shown before. As we know, PE segments own much faster nucleation rate than the PP segments; however, in the presence of amorphous random copolymers, their nucleation may be confined to some extent. As a result, the nucleation of PE segments will not influence the crystallization of PP segments. Under the ideal shear-enhanced crystallization model, the original multilayered phase structure has been destroyed by shear, and PE homopolymers have the chances to contact with ethylene–propylene block copolymer as well as PP homopolymers. Therefore, with the ceasing of shear and subsequent cooling, the shear-induced phase structure can be preserved and these crystallizable PE segments can also undergo normal crystallization and form perfect crystals. Because of the fast nucleation rate, the PE segments can provide sable nuclei for the subsequent crystallization of PP homopolymers, which results in the enhanced crystallization kinetic as observed. However, because of a self-recovery to the multilayered phase structure as we have shown, the shear-enhanced effect can be gradually suppressed by melt annealing. The solvent fractionation of IPC can be regarded as an extreme situation that the multilayered phase structure is totally destructed by removing the amorphous components, as illustrated in the globe lower-left in Figure 11A. The crystallizable PE segments are no longer trapped and can always gather together to undergo normal crystallization. Therefore, after solvent fractionation, the IPC sample owns a faster crystallization rate similar to the shear-enhanced situation. Moreover, this effect can never be suppressed even under melt annealing at high temperature. We have tried to keep the fractionationed IPC sample at 230 °C for 8 h, and the crystallization temperature did not show any changes, which strongly supported our explanation. Therefore, the model implies that there exists a dependence of shear rate in shear-enhanced crystallization of IPC due to the combination between the partially crystalline copolymer and the amorphous random copolymer. One may suggest that, according to the previous studies, the high molecular weight chains of iPP or PE will play a role in the shear-enhanced crystallization because they tend to form some precursors owing high melting temperature under shear which can act as nuclei for other components. We have discussed this explanation as you can see in the Supporting Information. We concluded that the shear-induced precursor may have an influence but apparently is not the main reason for the shear-enhanced crystallization in the present system.

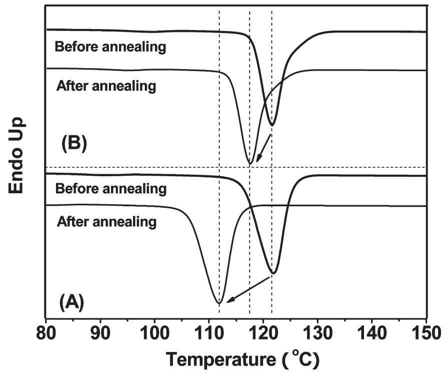

Figure 12. Crystallization curves of IPC-S (A) and partially fractionationed IPC-S (B) before and after annealing.

To further testify our model, we designed an experiment to partially remove the amorphous phase in IPC-S. From the model, it can be easily inferred that when part of amorphous components in IPC-S is removed, the possibility of a recovery of shear-enhanced crystallization still exists. However, the difference is due to the releasing of some block copolymer and PE chains from the amorphous phase; the enhanced crystallization cannot be completely eliminated. The partial removing of amorphous components can be realized in a convenient way. The IPC-S sample in its original solid form was directly fractionationed by *n*-hexane for a short time, and as a result, only the amorphous component close to the surface could be washed out. Figure 12 shows the crystallization curves of IPC-S and partially fractionationed IPC-S before and after same annealing procedure. From Figure 12, as we have expected, the crystallization behaviors of both samples exhibited recoveries back to their original states. For IPC-S samples, the T_p seemed to move to the value which was almost the same as IPC, indicating a sufficient relaxation of the unstable phase structure. However, with the same annealing procedure, the partially fractionationed IPC-S samples did not show a complete relaxation. The T_p only moved to a lower temperature but failed to reach the value of that of IPC. Moreover, it should be note that the loss of part of the amorphous components also lowers the possibility of the collision between block copolymers and random copolymers. To sum up, crystallization behavior of fractionationed IPC-S sample is nearly impossible to completely revert as predicted by our model.

In brief, the model of shear-enhanced crystallization in IPC we proposed here is based on the experimental results obtained and shows certain reasonableness from a macroscopic viewpoint. It should be admitted that, due to the complexity of IPC system, the detailed moving process of the chains in IPC under shear force still needs to be further explored in our future studies.

4. Conclusion

In this study, we have examined the shear-enhanced crystallization by a combinatory investigation of DSC, SEM, FETEM and POM techniques. The preshearing applied on iPP, iPP/EPR and IPC samples led to significantly accelerated crystallization kinetics only in IPC samples. It was found that this enhanced crystallization could be eliminated by suitable annealing procedures. Through FETEM observation, we have built up a multilayered phase structure of IPC. The phase morphology observed by SEM revealed that, in the case of IPC, the partially crystalline block copolymer works as a bridge connecting the dispersed amorphous phase and crystalline matrix, whereas in the case of IPC-S, this connection seemed to be destroyed. With the results of solvent and thermal fractionation, it was showed that both partially crystalline components and amorphous components play an important role in the shear-enhanced crystallization of IPC.

A model describing the mechanism of shear-enhanced crystallization in IPC was proposed. A correlation between the phase structure and corresponding crystallization behavior was constructed. According to the model, in IPC system, the PE homopolymers lie in the core area and are surrounded by amorphous ethylene−propylene random copolymers. The crystalline block copolymer with both crystallizable PP and PE segments exists as an interphase between the dispersed amorphous phase and the matrix. Crystallizable PP segments are inserted into the crystalline matrix while PE segments are trapped in amorphous phase. This multilayered phase structure is stable under a quiescent state. However, under the molten state, external shear can destroy the multilayered phase structure by pulling out PE homopolymers as well as the PE segments of block copolymers from amorphous phase. Because of the disconnection from the amorphous phase, the PE segments can gather together to form stable nuclei and play a role to enhance the subsequent crystallization rate of IPC by improving the nucleation rate. With annealing at high temperatures, both the shear-induced phase structure and shear-enhanced crystallization can be eliminated due to a spontaneous self-assembly back to the stable multilayered phase structure. It should also be noted that the shear-enhanced crystallization of IPC is accompanied by the destruction of original phase structure; that is, there exists the possible loss of original excellent balance between toughness and rigidity of IPC, which may be a potential problem in the processing of such materials.

Acknowledgment. We gratefully acknowledge the financial support from the Natural Science Foundation of China (Grants 50673021 and 20874017), the National Basic Research Program (G2005CB623803), and the National Hi-Tech Research & Development Program (2007AA03Z450).

Supporting Information Available: (1) POM micrograph of IPC-S crystallized at 150 °C; (2) WAXD result of IPC-S sample; (3) discussion about purpose of the pretreatment of IPC sample; (4) information about the molecular structure of soluble components in IPC; (5) discussion about the possible degradation and cross-linking of IPC sample during shearing; (6) discussion about the other possible explanation of shear-enhanced crystallization in IPC1. This material is available free of charge via the Internet at http://pubs.acs.org.

References and Notes

(1) Choudhary, V.; Varma, H. S.; Varma, I. K. *Polymer* **1991**, *32*, 2534–2540.
(2) Dorazio, L.; Mancarella, C.; Martuscelli, E.; Sticotti, G.; Massari, P. *Polymer* **1993**, *34*, 3671–3681.
(3) McNally, T.; McShane, P.; Nally, G. M.; Murphy, W. R.; Cook, M.; Miller, A. *Polymer* **2002**, *43*, 3785–3793.
(4) Pang, Y.; Dong, X.; Zhang, X.; Liu, K.; Chen, E.; Han, C. C.; Wang, D. *Polymer* **2008**, *49*, 2568–2577.
(5) Varga, J. *J. Macromol. Sci., Part B: Phys.* **2002**, *B41*, 1121–1171.
(6) Tjong, S. C.; Shen, J. S.; Li, R. K. Y. *Polym. Eng. Sci.* **1996**, *36*, 100–105.
(7) Zhao, S.; Cai, Z.; Xin, Z. *Polymer* **2008**, *49*, 2745–2754.
(8) Galli, P.; Vecellio, G. *Prog. Polym. Sci.* **2001**, *26*, 1287–1336.
(9) Galli, P.; Haylock, J. C. *Prog. Polym. Sci.* **1991**, *16*, 443–462.
(10) Simonazzi, T.; Cecchin, G.; Mazzullo, S. *Prog. Polym. Sci.* **1991**, *16*, 303–329.
(11) Wang, S.; Yang, D. *Polymer* **2004**, *45*, 7711–7718.
(12) Mirabella, F. M. *Polymer* **1993**, *34*, 1729–1735.
(13) Tan, H.; Li, L.; Chen, Z.; Song, Y.; Zheng, Q. *Polymer* **2005**, *46*, 3522–3527.
(14) Urdampilleta, I.; Gonzalez, A.; Iruin, J. J.; de la Cal, J. C.; Asua, J. M. *Macromolecules* **2005**, *38*, 2795–2801.
(15) Zheng, Q.; Shangguan, Y. G.; Yan, S. K.; Song, Y. H.; Peng, M.; Zhang, Q. B. *Polymer* **2005**, *46*, 3163–3174.
(16) Chen, Y.; Chen, Y.; Chen, W.; Yang, D. C. *J. Appl. Polym. Sci.* **2008**, *108*, 2379–2385.
(17) Chen, Y.; Chen, Y.; Chen, W.; Yang, D. C. *Eur. Polym. J.* **2007**, *43*, 2999–3008.
(18) Chai, C. K.; Auzoux, Q.; Randrianatoandro, H.; Navard, P.; Haudin, J.-M. *Polymer* **2003**, *44*, 773–782.
(19) Kumaraswamy, G.; Issaian, A. M.; Kornfield, J. A. *Macromolecules* **1999**, *32*, 7537–7547.
(20) Varga, J.; KargerKocsis, J. *J. Polym. Sci., Part B: Polym. Phys.* **1996**, *34*, 657–670.
(21) Somani, R. H.; Hsiao, B. S.; Nogales, A.; Srinivas, S.; Tsou, A. H.; Sics, I.; Balta-Calleja, F. J.; Ezquerra, T. A. *Macromolecules* **2000**, *33*, 9385–9394.
(22) Somani, R. H.; Hsiao, B. S.; Nogales, A.; Fruitwala, H.; Srinivas, S.; Tsou, A. H. *Macromolecules* **2001**, *34*, 5902–5909.
(23) Somani, R. H.; Yang, L.; Zhu, L.; Hsiao, B. S. *Polymer* **2005**, *46*, 8587–8623.
(24) Kumaraswamy, G.; Verma, R. K.; Issaian, A. M.; Wang, P.; Kornfield, J. A.; Yeh, F.; Hsiao, B. S.; Olley, R. H. *Polymer* **2000**, *41*, 8931–8940.
(25) Kumaraswamy, G.; Kornfield, J. A.; Yeh, F. J.; Hsiao, B. S. *Macromolecules* **2002**, *35*, 1762–1769.
(26) Vleeshouwers, S.; Meijer, H. E. H. *Rheol. Acta* **1996**, *35*, 391–399.
(27) Pogodina, N. V.; Lavrenko, V. P.; Srinivas, S.; Winter, H. H. *Polymer* **2001**, *42*, 9031–9043.
(28) Devaux, N.; Monasse, B.; Haudin, J. M.; Moldenaers, P.; Vermant, J. *Rheol. Acta* **2004**, *43*, 210–222.
(29) Liedauer, S.; Eder, G.; Janeschitzkriegl, H.; Jerschow, P.; Geymayer, W.; Ingolic, E. *Int. Polym. Process.* **1993**, *8*, 236–244.
(30) Janeschitz-Kriegl, H. *Macromolecules* **2006**, *39*, 4448–4454.
(31) Andersen, P. G.; Carr, S. H. *Polym. Eng. Sci.* **1978**, *18*, 215–221.
(32) Fritzsch, Ak; Price, F. P. *Polym. Eng. Sci.* **1974**, *14*, 401–412.
(33) Nogales, A.; Hsiao, B. S.; Somani, R. H.; Srinivas, S.; Tsou, A. H.; Balta-Calleja, F. J.; Ezquerra, T. A. *Polymer* **2001**, *42*, 5247–5256.
(34) Agarwal, P. K.; Somani, R. H.; Weng, W. Q.; Mehta, A.; Yang, L.; Ran, S. F.; Liu, L. Z.; Hsiao, B. S. *Macromolecules* **2003**, *36*, 5226–5235.
(35) Koscher, E.; Fulchiron, R. *Polymer* **2002**, *43*, 6931–6942.
(36) Huo, H.; Meng, Y. F.; Li, H. F.; Jiang, S. C.; An, L. J. *Eur. Phys. J. E* **2004**, *15*, 167–175.
(37) Chen, Q.; Fan, Y. R.; Zheng, Q. *Rheol. Acta* **2006**, *46*, 305–316.
(38) Wang, K.; Tang, C. Y.; Zhao, P.; Yang, H.; Zhang, Q.; Du, R. N.; Fu, Q. *Macromol. Rapid Commun.* **2007**, *28*, 1257–1264.
(39) Zhao, G. Y.; Zhang, M.; Men, Y. F.; Ding, M. X.; Jiang, W. *J. Polym. Sci., Part B: Polym. Phys.* **2007**, *45*, 2344–2349.
(40) Zhu, H. J.; Monrabal, B.; Han, C. C.; Wang, D. J. *Macromolecules* **2008**, *41*, 826–833.
(41) Zhang, X. H.; Wang, Z. G.; Muthukumar, M.; Han, C. C. *Macromol. Rapid Commun.* **2005**, *26*, 1285–1288.
(42) Shimizu, K.; Wang, H.; Wang, Z. G.; Matsuba, G.; Kim, H.; Han, C. C. *Polymer* **2004**, *45*, 7061–7069.
(43) Matsuba, G.; Shimizu, K.; Wang, H.; Wang, Z. G.; Han, C. C. *Polymer* **2004**, *45*, 5137–5144.
(44) Song, S. J.; Wu, P. Y.; Feng, J. C.; Ye, M. X.; Yang, Y. L. *Polymer* **2009**, *50*, 286–295.
(45) Muller, A. J.; Arnal, M. L. *Prog. Polym. Sci.* **2005**, *30*, 559–603.
(46) Janeschitz-Kriegl, H.; Eder, G. *J. Macromol. Sci., Part B: Phys.* **2007**, *46*, 591–601.
(47) Isayev, A. I.; Chan, T. W.; Shimojo, K.; Gmerek, M. *J. Appl. Polym. Sci.* **1995**, *55*, 807–819.
(48) Chai, C. K.; Dixon, N. M.; Gerrard, D. L.; Reed, W. *Polymer* **1995**, *36*, 661–663.
(49) Dai, W. L.; Liu, P. S.; Wang, X. Y. *J. Appl. Polym. Sci.* **2003**, *88*, 2784–2790.
(50) Azzurri, F.; Alfonso, G. C. *Macromolecules* **2005**, *38*, 1723–1728.

(51) Gutierrez, M. C. G.; Alfonso, G. C.; Riekel, C.; Azzurri, F. *Macromolecules* **2004**, *37*, 478–485.
(52) Muller, A. J.; Hernandez, Z. H.; Arnal, M. L.; Sanchez, J. J. *Polym. Bull.* **1997**, *39*, 465–472.
(53) Lorenzo, A. T.; Arnal, M. L.; Sanchez, J. J.; Muller, A. J. *J. Polym. Sci., Part B: Polym. Phys.* **2006**, *44*, 1738–1750.
(54) Kong, J.; Fan, X. D.; Xie, Y. C.; Qiao, W. Q. *J. Appl. Polym. Sci.* **2004**, *94*, 1710–1718.
(55) Mang, M. Q.; Wanke, S. E. *Polym. Eng. Sci.* **2003**, *43*, 1878–1888.
(56) Muller, A. J.; Arnal, M. L.; Spinelli, A. L.; Canizales, E.; Puig, C. C.; Wang, H. *Macromol. Chem. Phys.* **2003**, *204*, 1497–1513.
(57) Starck, P.; Rajanen, K.; Lofgren, B. *Thermochim. Acta* **2002**, *395*, 169–181.
(58) Zhang, F. J.; Fu, Q.; Lu, T. J.; Huang, H. Y.; He, T. B. *Polymer* **2002**, *43*, 1031–1034.
(59) Tribout, C.; Monasse, B.; Haudin, J. M. *Colloid Polym. Sci.* **1996**, *274*, 197–208.
(60) Hu, W. G.; Srinivas, S.; Sirota, E. B. *Macromolecules* **2002**, *35*, 5013–5024.
(61) Bracco, S.; Comotti, A.; Simonutti, R.; Camurati, I.; Sozzani, P. *Macromolecules* **2002**, *35*, 1677–1684.
(62) Lieser, G.; Wegner, G.; Smith, J. A.; Wagener, K. B. *Colloid Polym. Sci.* **2004**, *282*, 773–781.